Influence of carbon diffusion on microstructure and wear behaviour of duplex stainless steel surface layers on lamellar grey cast iron

Einfluss der Kohlenstoffdiffusion auf die Gefügeausbildung und das Verschleißverhalten von Duplexstahl-Auftragschweißungen auf Gusseisen mit Lamellengraphit

B. Heider[1], M. Oechsner[1], T. Engler[1], J. Ellermeier[1], U. Reisgen[2], R. Sharma[2], E. Zokoll[2], E. Gonzalez[2]

Surface welding with duplex stainless steel was performed to enhance the wear and corrosion properties of grey cast iron, which is used as material for applications as pump components in maritime and chemical environments. The method used for surface welding and the corresponding process parameters determine the chemical composition and microstructure, which both determine the corrosion and wear properties of the surface layer. High heat input leads to high chemical dilution and thus, reduced corrosion resistance. Slow cooling rates, which are recommended for welding of grey cast iron components, facilitate the formation of carbides in the fusion zone of the chromium-rich duplex stainless steel surface layer. On the one hand, carbides lead to increased hardness and thus, improved wear resistance of the surface layers. On the other hand, carbides and high chemical dilution rates reduce the corrosion resistance and therefore should be avoided. Under high cooling rates, the risk of cracking in the heat affected zone of the grey cast iron increases due to martensitic phase transformations. The paper describes the correlation of process parameters, microstructure and chemical composition with a focus on carbon diffusion and carbide formation, ever considering the effect on the wear behaviour in an oscillation tribometer and under erosion-corrosion conditions.

Keywords: Surface welding / carbon diffusion / phase formation / microstructure / abrasion wear / erosion-corrosion

Zur Erhöhung der Korrosions- und Verschleißbeständigkeit von Bauteilen aus Gusseisen mit Lamellengraphit, welches für Pumpenbauteile in beispielsweise Meerwasserumgebung oder chemischen Anlagen verwendet wird, wurden Auftragschweißschichten aus Duplexstahl hergestellt. Dabei bestimmen der Prozess des

[1] Zentrum für Konstruktionswerkstoffe (MPA-IfW Darmstadt), TU Darmstadt, Grafenstraße 2, 64283 DARMSTADT, FEDERAL REPUBLIC OF GERMANY
[2] Institut für Schweißtechnik und Fügetechnik (ISF) der RWTH Aachen University, Pontstraße 49, 52062 AACHEN, FEDERAL REPUBLIC OF GERMANY

Corresponding author: B. Heider, Zentrum für Konstruktionswerkstoffe (MPA-IfW Darmstadt), TU Darmstadt, Grafenstraße 2, 64283 DARMSTADT, FEDERAL REPUBLIC OF GERMANY,
E-Mail: heider@mpa-ifw.tu-darmstadt.de

Auftragschweißens sowie die entsprechenden Prozessparameter die chemische Aufmischung von Zusatz- und Grundwerkstoff sowie das resultierende Gefüge der Auftragschweißschicht. Die chemische Zusammensetzung und das Gefüge der Schicht bestimmen wiederum die Korrosions- und Verschleißbeständigkeit. Hohe Wärmeeinbringung bzw. Streckenenergie führt zu hoher Aufmischung und erhöhter Korrosionsanfälligkeit. Für das Schweißen von Gusseisen wird langsame Abkühlung empfohlen, während Duplexstähle unter solchen Bedingungen zur Ausbildung von versprödenden Phasen neigen. Auf der einen Seite steigern solche karbidischen Phasen die Härte der Duplexstähle und begünstigen damit die Verschleißbeständigkeit, auf der anderen Seite bilden diese Ausscheidungen Angriffspunkte für selektive Korrosion und verringern somit die Korrosionsbeständigkeit. Schnelle Abkühlung, die für das Schweißen von Duplexstählen empfohlen wird, erhöht wiederum besonders in der Wärmeeinflusszone des Graugusses das Risiko von martensitischen Umwandlungen, wodurch in dieser Zone Risse entstehen können. In diesem Manuskript wird der Zusammenhang zwischen Prozessparametern beim Auftragschweißen und der Aufmischung bzw. dem Gefüge und letztlich den sich daraus ergebenden Verschleißeigenschaften beschrieben. Ein besonderer Fokus liegt dabei auf dem Einfluss auf die Diffusion von Kohlenstoff und der Bildung von Karbiden.

1 Introduction

Surface welding is an established method to protect components from corrosion and wear, e.g. in the pump industry, where the corrosion resistance of austenitic stainless steel components is even enhanced by a welded surface layer of duplex stainless steels or nickel based alloys [1]. The excellent corrosion and wear properties of duplex stainless steels are achieved by high amounts of chromium and controlled balance of the ferrite-austenite ratio resulting from rapid cooling after annealing [2]. Both larger components as well as components with geometrical complexity to reduce the risk for erosion and cavitation phenomena aggravate this heat treatment [3]. For such components, e.g. impellers and pump casings, castable materials are the state of the art. There exist castable duplex stainless steels, however, the occurrence of detrimental phases, e.g. σ-phase is hardly avoidable [4]. An established and cheap material class for casting with beneficial damping characteristics are grey cast irons, but their resistance to corrosive media is poor [5]. Therefore, surface welding of duplex stainless steel on grey cast iron components promises a cost-efficient component with increased lifetime. Nevertheless, there are some not fully investigated and understood complications in welding of the material combination at hand.

Many researchers investigated the solidification mechanism and the resulting microstructure of various stainless steels depending on the cooling rate and optional post heat treatment of welded parts as well as the effects of artificial aging on the microstructure resulting in a deterioration of corrosion and mechanical properties. For instance, the chemical composition, namely an increase in nickel content has a much higher influence on the ferrite-austenite ratio than the cooling rate [6]. A higher carbon content as well as increasing nickel contents in the weld metal increase the austenite content, but increasing concentrations of carbon lead to decreasing corrosion resistance of the surface layers through formation of carbides [7, 8]. Carbidic phases are prominent for the use in a metal matrix for highly wear resistant materials and coatings due to their high hardness [9]. In a duplex stainless steel prepared by surface welding, such phases are unintended, but have to be considered, if the welding consumables are diluted with carbon from the grey cast iron substrate by the welding process. The question of interest to this research is how the carbon diffusion influences the phase precipitation and how this affects the mechanical-technological properties of the surface layer.

High cooling rates are inherent to the welding process, but - paired with melting and mixing of the materials - result in complications. Especially for the grey cast iron, rapid cooling may lead to martensite formation, which is usually suppressed in welding by preheating [10, 11]. But the consequently slower cooling rates and prolonged as well as repeated heat treatments facilitate the precipitation of detrimental phases in the (diluted) duplex stainless steel. These correlations and the mentioned influence on the wear properties are investigated in this study.

2 State of the art

2.1 Surface welding

Of various coating techniques, such as physical vapour deposition, chemical vapour deposition, thermal spraying or galvanizing, surface welding has the benefit of producing a tough, metallurgic bonding between the fusion zone and the parent material [7, 12–15]. The surface of the base metal is molten by an energetic beam and the welding consumable is applied on the surface to form the fusion zone. Surface welding can shape the dimensions of a component or enhance wear and/or corrosion properties of that component. Many welding techniques that differ in the type of heat source, the form of consumable and the power density distribution onto the substrate are available for surface welding, e.g. gas metal arc welding, plasma transferred arc welding or laser beam welding [9]. Shielding gases are used to protect the molten weld pool from oxidation. Shielding gases may be inert (e.g. argon, helium) or active (e.g. hydrogen, carbon dioxide). Preheating of the base metal decreases the cooling rates and reduces residual stresses in the surface layer and in the heat affected zone. One of the most important factors of surface welding is the chemical dilution that results from blending of the consumable with the parent metal in the fusion zone. A low chemical dilution is targeted to retain the chemical composition and the wear and corrosion properties of the selected consumable. The chemical dilution is inherent to welding and in combination with the heat input and diffusion in the surface layer, the microstructure of the surface layer changes.

2.2 Solidification of duplex stainless steels

Duplex stainless steels, such as the X2 CrNiMoN 22–5-3 are a class of material comprising both austenite and ferrite in a specific ratio and are tailored to excel at both corrosion and wear resistance [2]. The use of such steels is bound to a temperature range, e.g. 350 °C is a common upper limit for this alloy because brittle phases, such as the α'-phase may form and lead to deterioration of corrosion and mechanical properties (475 °C embrittlement) [16]. Other phases, e.g. σ-phase form if the steel is exposed to temperatures in the range of 800 °C-900 °C for extended durations. In a chemically pure duplex stainless steel, the σ-phase has to be considered if such high temperature are held for more than some 1000 h. But, as the phase formation is influenced by the chemical composition, which changes during welding, the time for precipitation of σ-phase and carbides can significantly decrease [17, 18]. Preheating reduces the cooling rates and thus, prolongs the duration at such temperatures and finally increases the risk of deleterious phases.

The solidification of the molten weld pool of a duplex stainless steel starts with the precipitation of δ-ferrite. Depending on the exact composition, austenite may also precipitate from the melt. Upon cooling, recrystallization and transformation of the δ-ferrite to secondary austenite takes place. The cooling rate determines the final microstructure: Very high cooling rates lead to a large portion of δ-ferrite, while at lower cooling rates, more δ-γ-transformation occurs and the portion of δ-ferrite decreases. The appearance of the austenite and remaining δ-ferrite varies a lot depending on the chemical composition and cooling rates. The ratio of chromium and nickel equivalent (Cr_{eq}/Ni_{eq}) is used to describe the microstructure that results from high cooling rates, e.g. up to 800 K s^{-1} in laser welding [8, 19–22]:

- $Cr_{eq}/Ni_{eq} > 1.95$: The melt solidifies purely to δ-ferrite. Upon cooling, δ-γ-transformation may occur. The resulting microstructure may be fully ferritic or contain austenite with a – according to contemporary literature – Widmanstätten appearance or acicular ferrite.
- $Cr_{eq}/Ni_{eq} < 1.95$: δ-ferrite precipitates primarily from the melt and upon further cooling the rest of the melt solidifies into ferrite and austenite. After solidification, δ-γ-transformation occurs.

The microstructure is composed of lacy ferrite or vermicular ferrite.

- $Cr_{eq}/Ni_{eq} < 1.48$: Eutectic solidification into both ferrite and austenite or austenite at first and then, ferrite occurs. The microstructure contains eutectic ferrite or intercellular / interdendritic ferrite.
- $Cr_{eq}/Ni_{eq} < 1.25$: The solidification is purely austenitic and no transformation occurs upon cooling.

Therefore, a higher Cr_{eq}/Ni_{eq} equivalent supports ferrite formation from the melt and if high enough, the δ-γ-transformation may even be suppressed. In order to achieve the properties of duplex stainless steel, a well-balanced phase distribution is required, so for high Cr_{eq}/Ni_{eq} equivalents the cooling rate has to be low to enable the δ-γ-transformation.

3 Aim of the investigation

The combination of a cost efficient material for pump components with an enduring surface layer is of interest for industrial application but poorly understood in fundamental research. Several challenges exist in surface welding of grey cast iron with duplex stainless steel. The chemical composition of a stainless steel and the cooling rate determine the resulting microstructure of the surface layer, but this is subjected to considerable changes through chemical dilution during surface welding. Most importantly, the recommended welding procedures are very different for both materials, i.e. duplex stainless steels should be solution annealed followed by water quenching while grey cast irons should be preheated to high temperatures and cooled down very slowly. For instance, surface

welding of grey cast iron without preheating is prone to the formation of brittle martensitic and ledeburitic phases in the heat affected zone and the partial fusion zone that may eventually lead to cracking. At the same time, preheating, slow cooling rates as well as increased chemical dilution will promote the precipitation of detrimental phases in the surface layers. The chemical dilution of duplex stainless steel with grey cast iron will lead to altered Cr_{eq}/Ni_{eq} ratios in the resulting fusion zones and different heat inputs during welding will alter the cooling rate. The aim of the investigation is to develop an understanding of the microstructural evolution in the fusion zone depending on the surface welding parameters energy input and cooling rate that both lead to changes in chemical dilution and varying degrees of diffusion. Furthermore, the influence of the microstructure in the fusion zone on the wear properties under oscillatory and erosive-corrosive loading is investigated.

4 Materials and experimental details

4.1 Materials

The substrates for surface welding are plates of lamellar grey cast iron EN-GJL-250 according to DIN EN 1561:2012-01 with dimensions (*w* x *l* x *h*) 200 mm x 300 mm x 8 mm [23]. The microstructure is pearlite and ferrite with embedded graphite flakes.

The welding consumables have a chemical composition close to that of X2 CrNiMoN 22–5-3 (1.4462), *Table 1*. A larger deviation from the nominal composition is found for the wire used for gas

Table 1. Chemical composition determined by spark optical emission spectroscopy, and chromium and nickel equivalents of grey cast iron and the consumables for gas metal arc surface welding GMA-SW (wire) and plasma transferred arc surface welding PTA-SW (powder). Duplex stainless steel composition range is extracted from data sheet following [26] DIN EN 10088–3:2014-12.

	C [wt %]	Si [wt %]	Mn [wt %]	P [wt %]	S [wt %]	Cr [wt %]	Mo [wt %]	Ni [wt %]	N [wt %]	Fe [wt %]	Cr_{eq} [%]	Ni_{eq} [%]
EN-GJL-250	3.43	1.94	0.76	0.06	0.19	0.11	0.04	0.1	-	92.0	3.1	103
X2 CrNiMoN 22-5-3	≤ 0.03	≤ 1.0	≤ 1.69	≤ 0.035	≤ 0.015	21.0 -23.0	2.5 - 3.5	4.5 - 6.5	0.1 - 0.22	Balance	25.6	10.3
GMA-SW wire	0.022	0.49	1.69	0.01	<0.01	22.7	3.14	8.73	0.146	62.9	26.6	10.3
PTA-SW powder	0.029	0.76	1.20	0.02	0.00	23.4	3.22	5.66	0.150	65.3	27.8	7.14

metal arc welding: The mass concentration of nickel is higher. This increases the nickel equivalent, countering the high cooling rates to support the formation of austenite. Depending on the dilution with grey cast iron in the fusion zone, the mass concentration of elements with a positive effect against corrosion (chromium, nickel, molybdenum and nitrogen) will decrease while the mass concentration of iron will increase and thus, the corrosion resistance of the surface layer may decrease. It is thus essential to minimize the chemical dilution of the fusion zone with grey cast iron elements. To estimate the microstructure, the chromium and nickel equivalents were calculated by Schaeffler equations (1) and (2), Table 1.

$$\%Ni_{eq} = \%Ni + 30 \cdot \%C + 0.5 \cdot \%Mn \quad (1)$$

$$\%Cr_{eq} = \%Cr + \%Mo + 1.5 \cdot \%Si + 0.5 \cdot \%Nb \quad (2)$$

For gas metal arc surface welding, a wire with a diameter of 1.0 mm and for plasma transferred arc surface welding a powder with a particle size distribution $-150 + 53$ μm is chosen [24, 25].

4.2 Surface welding and sample extraction

Two methods that differ in their arc characteristics, power density and heat input into the base metal are used for surface welding: Gas metal arc surface welding (GMA-SW) and plasma transferred arc surface welding (PTA-SW). For both methods, argon is used as inert shielding gas.

In gas metal arc surface welding, the arc is ignited between a consumable wire electrode and the base metal. Typically, the arc can be described as a paraboloid 45° with a basal plane diameter of 4 mm - 5 mm on the surface of the base metal, *Figure 1*a. A specialty of the used cold metal transfer (CMT) process is that during droplet detachment, the current is reduced to a minimum and the wire feed direction is reversed. This leads to an optimized energy input, less spatter and penetration and eventually, a reduced chemical dilution of the fusion zone [27]. The interplay between the melting wire electrode and the stability of the free-burning arc in gas metal arc welding strongly depends on
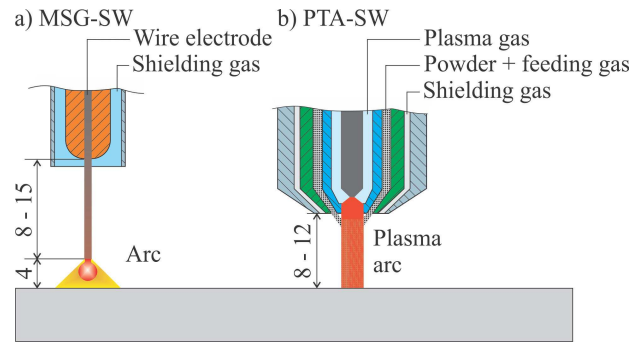

Figure 1. Schematic depiction of the formation of a) the free-burning arc between the consumable wire electrode and the base metal in gas metal arc surface welding and b) the plasma arc between the non-consumable tungsten electrode and the base metal in plasma transferred arc surface welding. Dimensions are given in mm.

the respective regulation strategy and the implemented parameter set (synergic line) and is a drawback compared to welding processes with non-consumable electrodes: The current that provides the arc with sufficient heat to melt the surface of the base metal also melts the wire electrode and controls the arc stability as well.

In plasma transferred arc surface welding, the non-transferred arc is ignited between a non-consumable tungsten electrode in the torch and the plasma gas nozzle to ionize the plasma gas. A homogeneously distributed high power density is a characteristic of this nearly cylindrical arc. Depending on the orifice diameter of the nozzle and the tungsten electrode diameter it has a typical diameter of a few millimeters, Figure 1. In contrast to gas metal arc surface welding, this configuration allows a more independent adjustment of heat input and powder feed rate.

The electrical welding parameters are kept constant and only the preheating temperature is varied, *Table 2*. Each set of electrical parameters was optimized to minimum chemical dilution (without preheating). In contrast to plasma transferred arc surface welding, the effect of the cold metal transfer technology is expressed by a variation of current and voltage: To maintain process stability, current and voltage are adjusted by the control unit in the current source.

The base metal plates are clamped onto a heating device for preheating. On the one hand, preheating will increase the chemical dilution because of a higher bias heat input to the grey cast iron,
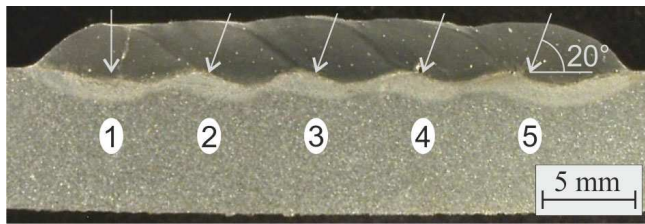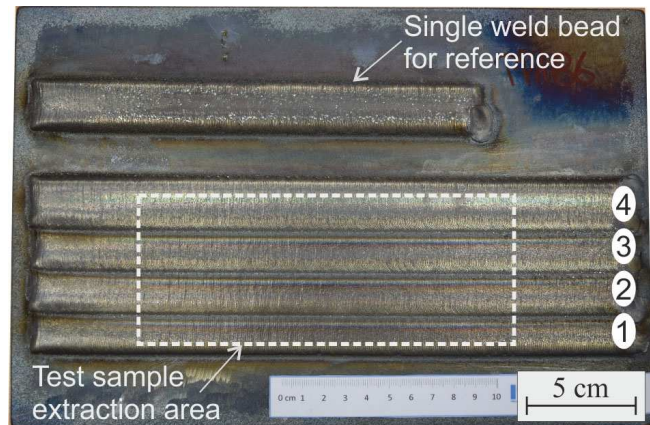
Figure 2. Cross-section of a surface layer consisting of five weld beads produced with gas metal arc surface welding without oscillation. First weld bead without torch inclination, second to fifth weld bead with 20° torch inclination to produce a smooth surface.

Figure 3. A surface layer consisting of 4 weld beads and a single weld bead for reference on a grey cast iron plate prepared by plasma transferred arc surface welding. The test samples were extracted from the center of the surface layer area by water jet cutting.

greater penetration and higher fluidity of the molten pool. The dilution changes the chemical composition and the microstructure of the surface layers which is likely to alter the corrosion and wear behaviour. On the other hand, preheating will lead to decreased cooling rates, thus longer cooling times and variations in phase precipitation and transformation. Lower cooling rates by preheating are supposed to suppress martensitic transformation, decrease the hardness in the heat affected zone and reduce the risk of cracking.

To produce the surface layers, the weld beads are aligned in parallel with an offset that is adapted to the single weld bead width. This offset is chosen as a compromise between sufficient overlap and smooth surface appearance. In gas metal arc surface welding, the torch is tilted to an angle of 20° to produce the smooth surface, *Figure 2*.

To obtain test samples for corrosion and wear tests as well as for metallographic investigations,

surface layers with dimensions of approx. (*w* x *l*) 90 mm × 280 mm are welded on the grey cast iron plates, *Figure 3*. The thickness of the surface layers is approx. 3 mm‐4 mm. After welding, the plates with surface layers cool down at ambient conditions. Round, disk like test samples are extracted from the center of the surface layer by water jet cutting. It is ensured that samples for metallographic investigation, chemical analysis and corrosion and wear testing originate from similar regimes, i.e. samples from the first welding passes are taken for valid comparability. The surface of the samples is smoothened by grinding with silicon

Table 2. Process parameters used for gas metal arc surface welding (GMA-SW) and plasma transferred arc surface welding (PTA-SW).

Process	Current [A]	Voltage [V]	Travel speed [cm min⁻¹]	Preheating temperature [°C]	Plasma gas flow [l min⁻¹]	Shielding gas flow [l min⁻¹]	Feeding gas flow [l min⁻¹]	Wire feeding rate [m min⁻¹]	Torch distance [mm]	Deposition rate [kg h⁻¹]
GMA-SW	102.0	12.9	40	25	-	18	-	7	14	2.6
GMA-SW	117.6	17.3	40	400	-	18	-	7	14	2.6
PTA-SW	149.1	19.5	5	25	0.5	10	3	-	5	1.4
PTA-SW	149.1	19.2	5	200	0.5	10	3	-	5	1.4
PTA-SW	149.2	19.2	5	400	0.5	10	3	-	5	1.4

carbide papers to allow determination of e. g. abrasion volume and erosion depth.

4.3 Chemical composition and microstructure of the surface layer

The chemical composition and the cooling rate determine the solidification, subsequent solid state transformation and thus, the final microstructure which, in an interplay with the chemical composition, influences the mechanical-technological properties as well as the corrosion resistance of the surface layers. Several techniques are applied to investigate both chemical composition and microstructure.

To determine the chemical composition, spark optical emission spectroscopy (OES) is used. The measurement is performed at 3-4 areas on ground (600-grit) surface layers with a spot size of approx. 4 mm and a penetration depth of approx. 0.1 mm. The following equation (3) provides the chemical dilution of any element in the surface layer using the concentration of that element in the fusion zone x_i, in the base metal x_B and in the welding consumable x_W [28,29]. The overall chemical dilution of each surface layer is determined as the average dilution of selected elements iron, chromium and nickel.

$$\% \, Dilution \; = \; \frac{x_i - x_W}{x_B - x_W} \cdot 100 \; \% \tag{3}$$

Cross-sections of the samples are prepared to investigate the microstructure using light microscopy (Leica DM 4000 M). Etching of the fusion zones with Groesbeck's reagent reveals the microstructure: Carbides are etched strongly and ferrite is etched lightly while austenite is not attacked by that etching agent and appears white in the microstructure. The image processing software Fiji is used to determine the austenite amounts by color thresholding.

Additionally, the fusion zones are investigated by X-ray diffractometry (Bruker D8 Advance). The intensity is measured in a 2θ-range of 10°-100° with a stepwidth of 0.0066°, a scan speed of 0.0132° s^{-1} and a spot size of 6 mm with a rotating sample. The acceleration voltage is 30 kV and acceleration current is 40 mA on a copper anode. The Cu-K$_\alpha$-wavelength of 0.15418 nm is used to determine the diffraction spectrum.

4.4 Mechanical-technological properties

The chemical composition and the microstructure influence the hardness of the fusion zones and thus, their resistance against abrasion and erosion.

According to DIN EN ISO 9015-1:2011-05 and DIN EN ISO 9015-2:2016-10 a test load of 49.03 N (HV 5) is used to determine the Vickers hardness of the fusion zones prepared with both gas metal arc surface welding and plasma transferred arc surface welding [30,31]. To avoid surface effects as well as influences between the individual indentations, a distance of 0.5 mm to the surface is kept and five indentations are made.

The wear tests are performed using an oscillation tribometer (SRV®3, Optimol Instruments). The round sample is mounted on a heated sample stage (30 °C) and an aluminum oxide ball counterpart of 10 mm diameter is used to apply the normal force on the sample surface which is ground with 400-grit silicon carbide grinding paper prior to mounting. Oscillation of the counterpart is performed at ambient humidity for 100 000 cycles at a frequency of 20 Hz, amplitude of 0.75 mm, and normal force of 20 N, which corresponds to a Hertzian pressure of approx. 1.5 GPa [32]. The friction coefficient is recorded and after the test, the wear track appearances of the sample and the counterpart are documented and the lateral extensions measured by digitally instrumented macroscope (Wild M 400, Wild Heerbrugg). The maximum depth of the wear track of the sample is determined by profilometer (T 8000, Jenoptik) and the total wear volume (sample and counterpart) is calculated according to DIN 51834-2:2010-11 and DIN 51834-3:2008-12 [33,34].

The erosion tests are performed in a test rig designed to produce a service-like erosive-corrosive loading which is able to provide qualitatively comparable results [35]. Four samples may be tested at the same time. To check for reliability and comparability of the individual erosion tests, one sample of duplex stainless steel (X2 CrNiMoN 22-5-3, 1.4462) is built into the test rig ever at the same position and controlled for constant wear. In that setup, a ceramic impeller is rotated at 1400 min^{-1} to

propel a mixture of fluid (artificial sea water according to DIN 50905-4:2008-12) and solid particles (aluminum oxide) onto the surface of the samples [36].

The rotational movement of the impeller creates a flow of approx. 15.5 m s^{-1} at an impact angle of approx. 30° relative to the sample surface [37]. That angle and the geometric constrictions of the sample holder result in a horizontally graded damage profile on the sample surface. The erosion tests are performed for 200 h in 10 intervals of 20 h, after which the test fluid (3.5 l) and solid particles (100 g l^{-1}) are renewed. After the tests, the erosion depth profiles along the horizontal axis are determined by a profilometer to quantify and compare the erosion damage between the surface layers. Metallographic cross-sections along the same axis are prepared to investigate the erosion mechanism.

5 Results and discussion

5.1 Chemical composition and microstructure of the surface layer

The chemical composition is of high importance, because the increase or decrease of chemical elements that stabilize either austenite or ferrite will determine the microstructure and eventually determine the wear and erosion resistance of the resulting surface layer.

The chemical dilution of the fusion zones prepared with plasma transferred arc surface welding without preheating and with 200 °C preheating temperature is so low (2.0 % and 3.3 %) that it almost matches the composition of the consumable, Table 1, *Table 3*. For gas metal arc surface welding without preheating temperature results a higher di-

lution (3.5 %) compared to plasma transferred arc surface welding. With 400 °C preheating temperature applied during gas metal arc surface welding, the dilution increases up to 16.9 %. At similar preheating temperatures, a higher dilution (22.6 %) is produced by plasma transferred arc surface welding.

The concentrations in the fusion zone of duplex stainless steel alloying elements chromium, molybdenum, nickel and nitrogen decrease with increasing dilution while the concentrations of iron and carbon increase due to their relatively higher content in the base metal. Deviations, for instance in the manganese and nickel concentrations, result from the different composition of the welding consumables, Table 1.

The chromium and nickel equivalents and their ratios were calculated according to equations (1) and (2) to estimate the solidification mode, *Table 4*. After solidification, every element takes influence on the formation and stability of phases in its own way. For instance, carbon has a high tendency to stabilize austenitic phases, however, the high affinity to chromium which may lead to formation of chromium carbides may be of higher importance considering the wear and erosion properties.

To investigate the microstructure, cross-sections were prepared and etched with Groesbeck's etchant for metallographic analysis. This reagent leaves austenite pristine while it etches carbides as well as σ-phase strongly and ferrite less strongly, *Figure 4*. From this, information about solidification and solid state transformation of the fusion zones may be deduced.

For the fusion zones with 2.0 % and 3.3 % dilution that have a Cr_{eq}/Ni_{eq} much greater than 1.95, the solidification was purely ferritic. Upon cooling, austenite precipitated at the grain boundaries,

Table 3. Dilution and chemical composition determined by spark optical emission spectroscopy of the surface layers prepared by plasma-transferred arc surface welding (PTA-SW) and gas metal arc surface welding (GMA-SW) sorted by ascending dilution.

Process	Preheating [°C]	Dilution [%]	C [wt %]	Mn [wt %]	Cr [wt %]	Mo [wt %]	Ni [wt %]	N [wt %]	Fe [wt %]
PTA-SW	-	2.0	0.022	1.10	22.5	3.17	5.75	0.193	66.2
PTA-SW	200	3.3	0.051	1.07	22.1	3.12	5.70	0.189	66.6
GMA-SW	-	3.5	0.128	1.64	21.9	3.07	8.44	0.133	63.9
GMA-SW	400	16.9	0.564	1.49	18.9	2.57	7.34	0.112	68.1
PTA-SW	400	22.6	0.475	0.98	17.8	2.41	4.67	0.127	72.2

Table 4. Chromium and nickel equivalents, and determined austenite content of the fusion zones, and the respective surface welding parameters sorted by ascending dilution. The austenite content was determined by digital image analysis (color thresholding) of etched micrographs of the fusion zones.

Process	Preheating [°C]	Dilution [%]	Cr_{eq} [%]	Ni_{eq} [%]	Cr_{eq} / Ni_{eq}	Austenite [%]
PTA-SW	-	2.0	26.6	7.0	3.8	46.4
PTA-SW	200	3.3	26.3	7.8	3.4	47.0
GMA-SW	-	3.5	25.8	13.1	2.0	67.3
GMA-SW	400	16.9	22.6	25.0	0.9	92.6
PTA-SW	400	22.6	21.6	19.4	1.6	73.9
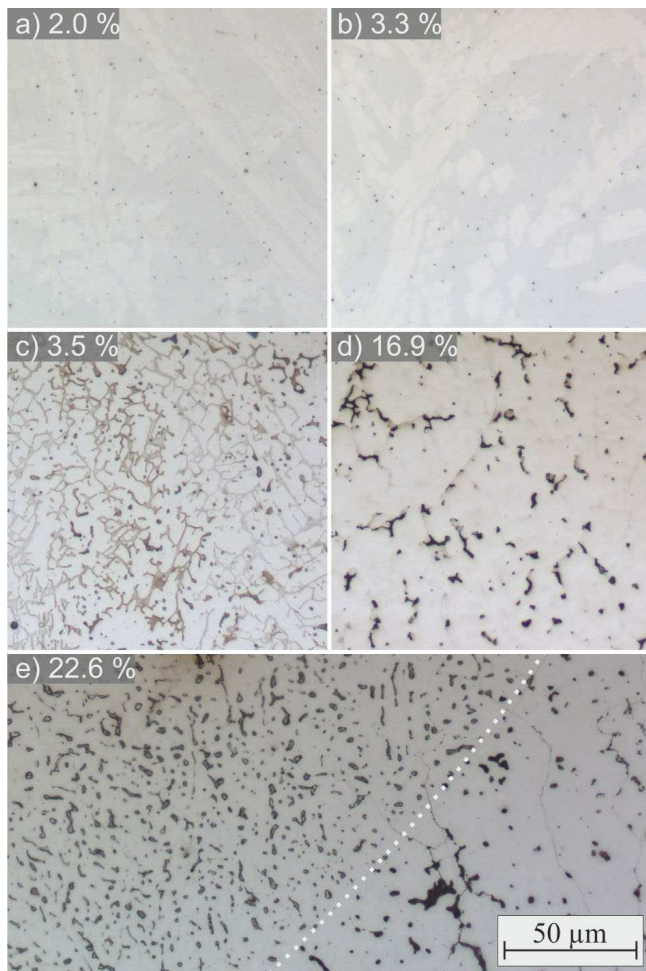
Figure 4. Cross-sections of the fusion zones with different dilution at x500 magnification. The cross-sections were etched with Groesbeck's reagent to show the microstructure. Carbide is attacked heavily, ferrite is attacked to a lesser degree and austenite is not attacked. At e), a dotted line indicates the border between two adjacent weld beads.

which resulted in austenite in a ferrite-matrix with an appearance that is sometimes mentioned to be similar to Widmannstätten, Figure 4a, b [8, 38]. After cooling, the microstructure of the fusion zone

with 2.0 % dilution comprises 46.4 % austenite, while the fusion zone with 3.3 % contains a slightly higher 47.0 % austenite, according to a lower Cr_{eq}/Ni_{eq} as well as reduced cooling rates, Figure 4, Table 4. The applied preheating temperature of 200 °C was low enough to maintain sufficiently high cooling rates that prevented any major δ-γ-transformation. The dilution was low and cooling rates were too high for precipitation of any significant amounts of carbides, i.e. the diffusion times and rates were negligible in that aspect.

With a higher dilution of 3.5 %, corresponding to a Cr_{eq}/Ni_{eq} of 2.0, the initial solidification was fully or almost fully ferritic. The resulting microstructure of the fusion zone comprises ferrite and 67.3 % austenite, Figure 4c. This means that during the cooling of the surface layer, a large portion of the solidified material could transform into austenite. The reason for this is the broadened heat distribution caused by the wide opening angle of the arc and the heat conductivity of the shielding gas: As the torch moves further, the solidifying weld still receives some heat and cooling rates are reduced. This enables the δ-γ-transformation in the microstructure: Diffusion times are longer and carbon can diffuse into an austenite matrix, where its solubility is higher.

At higher dilution of 16.9 %, the Cr_{eq}/Ni_{eq} is 0.9 and the solidification happened fully or almost fully austenitic. The nickel equivalent is high, the heat influence by the arc in gas metal arc surface welding is large and thus, the final microstructure contains 92.6 % austenite, Figure 4d. There are some dispersed precipitates in the microstructure which are most likely carbides or σ-phase. These could form because of enhanced diffusion through extended time at high temperatures and reduced cool-

ing rates caused by the preheating temperature of 400 °C.

At the highest dilution of 22.6 %, and a similar Cr_{eq}/Ni_{eq} of 1.6 (the similarity is caused by the differences in the chemical composition of the feedstock materials, Table 1), the microstructure formation was much like the former. In comparison to the fusion zone with 16.9 % dilution, this one has a lower austenite content of 73.9 %. At the transition between two adjacent plasma transferred arc weld beads, two regions were identified, Figure 4e: In the weld bead to the right (the earlier surface welded bead), grain coarsening happened in consequence to the heat-treatment by the later surface welded bead. Additionally, for the same reason, carbides have formed in that area. In the weld bead to the left, there seems to be a microstructure with more ferrite, comparable to the fusion zone from gas metal arc surface welding with 3.5 % dilution. The explanation for these microstructural differences is that the left weld bead has been surface welded on top of the earlier welded bead. This may lead to a dilution locally lower than 22.6 %, thereby increasing the Cr_{eq}/Ni_{eq} to numbers at which the solidification must have happened partly ferritic, but carbide precipitates are already observed at the austenite-ferrite interfaces.

The results of the metallographic analysis of the cross-sections of the fusion zones after etching with Groesbeck's reagent were confirmed by X-ray diffractometry, *Figure 5*. The diffractograms of fusion zones with 2.0 % and 3.3 % as well as 3.5 % show peaks of both austenite and ferrite, while the diffractograms of fusion zones with 16.9 % and 22.6 % show only peaks of austenite.
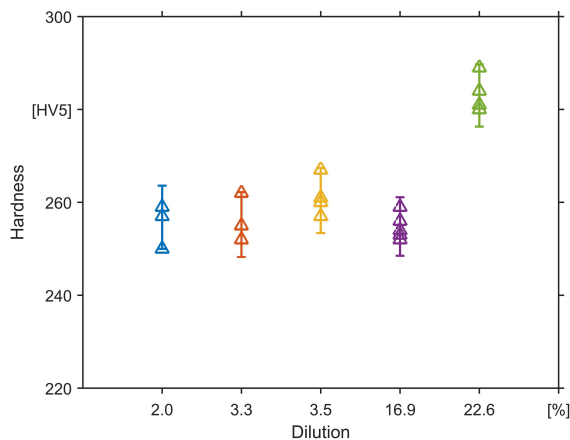
The Vickers hardness HV 5 of the fusion zone was determined as the average of five indentations made in the cross-sections of the samples. After the indentations, the samples were etched with Groesbeck's reagent to investigate the microstructure. Overall, the fusion zones with 2.0 % to 16.9 % dilution have similar mean hardness between 254.8 HV 5 for 16.9 % dilution and 260.4 HV 5 for 3.5 % dilution, *Figure 6*. A higher hardness of 283.0 HV 5 was determined for the fusion zone with 22.6 % dilution in the region of the first weld bead which had higher carbide content compared to the second weld bead, Figure 4e.

5.2 Mechanical properties

The mechanical properties are impacted by the dilution and the local microstructure. A higher dilution as well as longer cooling times, i.e. lower cooling rates, influence the solidification mode and the solid state transformation and thus, the final microstructure in the fusion zone. Especially through application of preheating temperature, the dilution increases and e.g. carbon diffusion is enhanced. This may increase the austenite content, but this may also facilitate the formation of carbides. A duplex stainless steel gets its excellent wear properties from a well-balanced phase ratio of austenite to fer-
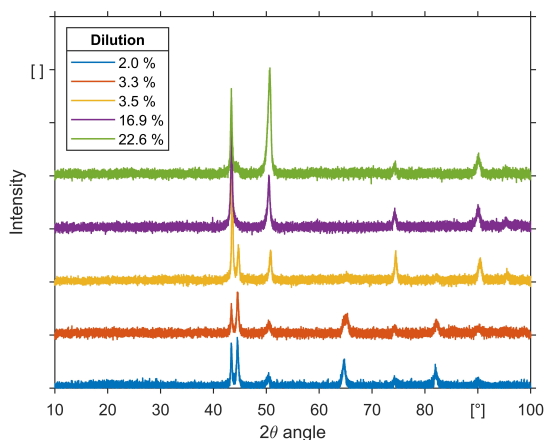
Figure 5. X-ray diffractograms of the fusion zones with different dilution. The intensities are background-corrected and shifted vertically to facilitate discrimination.


Figure 6. Vickers hardness HV 5 of the fusion zones with different dilution with error bars indicating the standard deviation of five measurements.

rite, so variations in the phase ratio and the presence of additional phases will affect both the hardness and the resistance against wear and erosion. Corrosion tests have shown that the phase boundaries between carbide precipitates and surrounding austenite matrix are critical for the initiation of intergranular corrosion. Surface layers with evenly distributed austenite and ferrite in the fusion zone however, show excellent corrosion behavior [7, 15].

5.2.1 Oscillation tests

The resistance against abrasion in dry condition was investigated with an oscillation tribometer with an aluminum oxide ball as counterpart. Here, the results of 20 N normal force, 20 Hz oscillation frequency, 0.75 mm stroke amplitude after 100 000 cycles at 30 °C temperature are presented. The friction coefficient was recorded and the total wear volume (ball and sample) after the test was determined by combination of optical and tactile methods.

The friction coefficient typically increased in the first 10 000 - 20 000 cycles of the test, after which it was stable around a value of 1.1 - 1.2, *Figure 7*. This initial increase is attributed to smoothening of surface asperities, which increases the contact area. After that smoothening, some transient changes in the friction coefficient occur, which may result from abrasive or adhesive phenomena, e. g. an increase in the friction coefficient may result from a
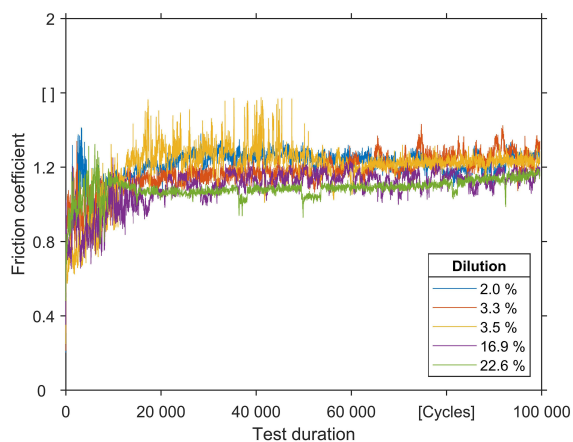
debris particle in the oscillation path. Overall, the evolution of the friction coefficients during oscillation of the aluminum oxide ball against the individual surface layers with different dilution does not vary much. It is arguable to say that with 16.9 % and 22.6 % dilution the friction coefficients are slightly lower, which may be due to the higher carbon content that can act as a solid lubricant.

The total wear volume of the aluminum oxide ball and the surface layer decreases with increasing dilution, i. e. higher dilution seems to have a beneficial effect on the abrasion resistance, *Figure 8*.

The surface layer with 2.0 % dilution has the highest wear loss, followed closely by the surface layers with 3.5 % and 3.3 % dilution. The wear volume of the surface layer with 16.9 % dilution is approx. half of that and the surface layer with 22.6 % dilution has the lowest wear loss. This trend can not be explained conclusively with an increase in hardness, Figure 6, 8. Such a relation would be expected for the case of purely abrasive loading, however, the high Hertzian pressure and the oscillation induce also a fatigue loading as well as plastic deformation on the surface. In contrast to that, there is a significant influence of the microstructure on the wear mechanism. For instance, the microstructure of the surface layer with 2.0 % dilution comprises evenly balanced austenite and ferrite, while for increasing dilutions, there are also carbides in the microstructure. Ferrite is – according to literature – softer than austenite, but carbides are much harder.
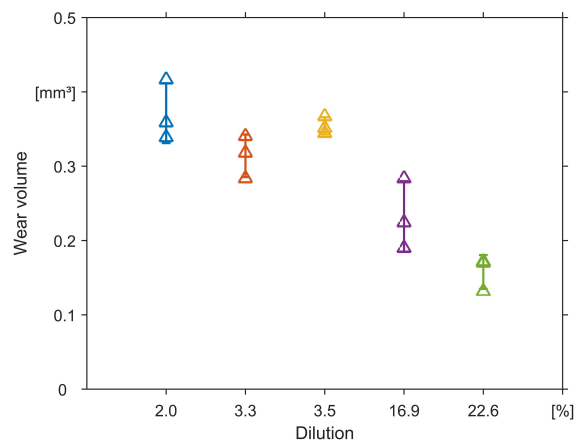

Figure 7. Evolution of the friction coefficient during oscillation test of aluminum oxide ball against the surface layers with different dilution over the duration of 100 000 cycles.
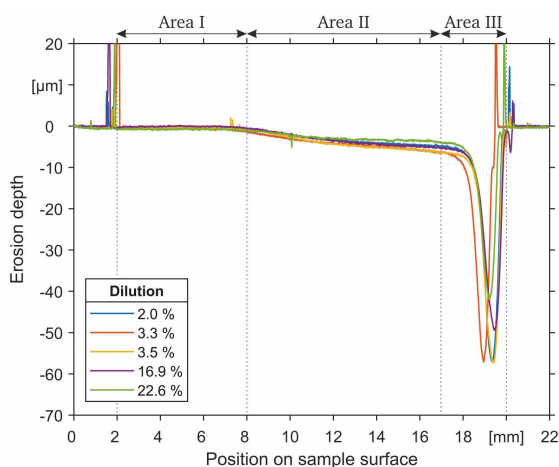

Figure 8. Wear volume after 100 000 cycles of oscillation test at 20 N normal force with aluminum oxide ball against the surface layers with different dilution with error bars indicating the standard deviation of three tests.

So one important microstructural aspect is dispersion hardening, the other is solid solution hardening in the austenite. A higher amount of ferrite therefore leads to decreased abrasion resistance, while an increasing amount of carbides embedded in the surface layer increases the abrasion resistance. The carbide network which comprises the microstructure of the surface layer with 22.6 % dilution reduces the overall ductility – thereby reducing plastic deformation – and eventually leads to the highest increase in abrasion resistance.

5.2.2 Erosion-corrosion tests

The resistance against erosion-corrosion in a mixture of artificial seawater with aluminum oxide particles was investigated and the results are qualitatively compared with use of the erosion depth profiles after the test, that reveal the amount of eroded material, *Figure 9*. The first and last 20 mm each correspond to the sample surface not exposed to the erosion loading. A clearly identifiable peak which corresponds to adhesive debris that was collected at the sealing ring marks the border to the erosive-corrosively loaded area. In that area, three zones may be distinguished. Going from left to right, there is the first area where no material was eroded (2 mm‑8 mm), the second area where moderate erosion occurred (8 mm‑17 mm) and the third area where material was heavily eroded and which is called the erosion trench (17 mm‑20 mm).

The very aggressive erosion conditions in the third regime are a result of the geometrical boundaries produced by the fluid-solid particle flow and the sample holder: The mixture of fluid and solid particles is accelerated into the edge that is formed by the sample surface and the sample holder and through this, additional vortices are created that cause the highest erosion rate on the material. A portion of the erosion depth profile of the second and third regime clearly shows the depth of the erosion trench, *Figure 10*. Lower erosion depth corresponds to higher erosion resistance, so with approximately 40 µm erosion depth, the surface layer with 22.6 % dilution provides the most erosion resistance, followed by the surface layer with 16.9 % dilution at approximately 50 µm erosion depth. The deepest erosion trenches, i.e. the highest erosion damage are detected for the surface layers with 2.0 %, 3.3 % and 3.5 % dilution with similar values for the erosion depth of about 60 µm.

To investigate the damage mechanism, cross-sections of the samples along the erosion depth profile were prepared and surveys of the erosion trench and details in the deepest damaged area were recorded, *Figure 11*. The contour of the erosion trenches is smooth, meaning there is no heigth difference between the various occuring phases austenite, ferrite, σ-phase and carbides. This is true for all samples with the different dilutions and microstructures. The chemical dilution of the duplex stainless steel surface layers does not aggravate the resistance against the combined erosion-corrosion

Figure 9. Erosion depth profiles after 200 h erosion test of the surface layers with different dilution.
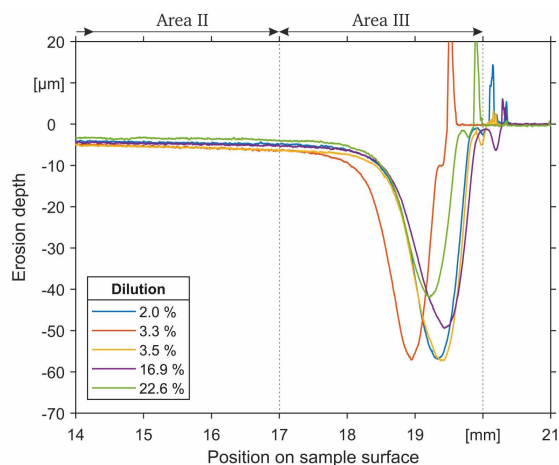
Figure 10. Erosion depth profiles zoomed on the erosion trench after 200 h erosion test of the surface layers with different dilution.
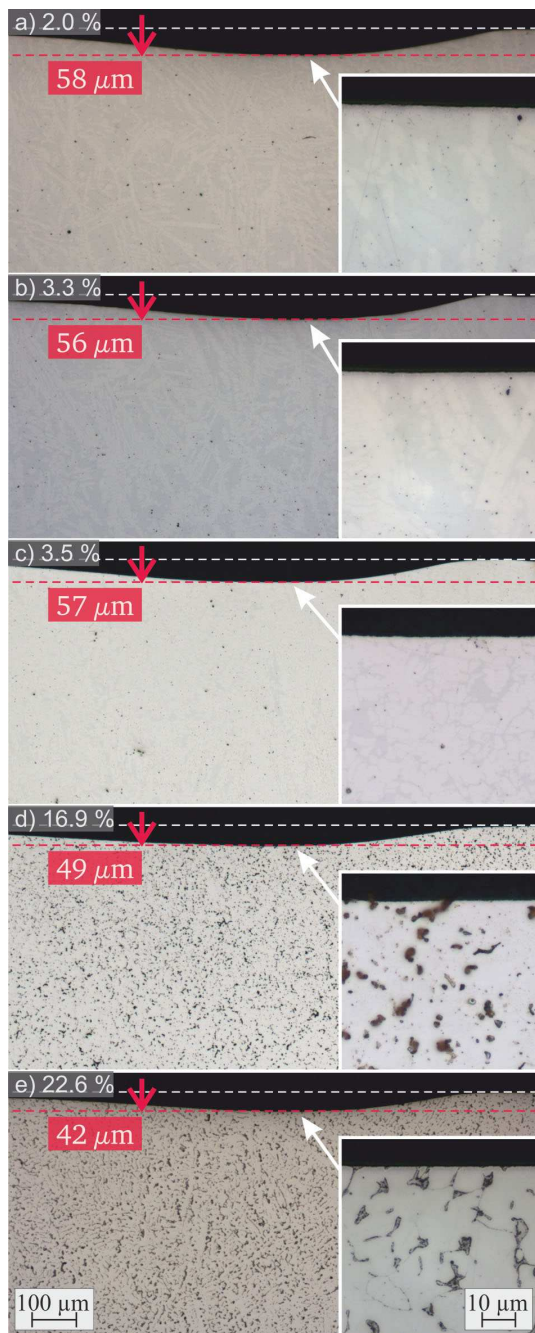
Figure 11. Cross-sections of the erosion trenches of the fusion zones after 200 h erosion test of the surface layers with different dilution at x100 magnification and x1000 magnification (insets). The cross-sections were etched with Groesbeck's reagent to show the microstructure.

loading. Instead, the increased chemical dilution that leads to precipitation of σ-phase and carbides as well as solid solution hardening and dispersion hardening has a positive effect on the resistance against erosion-corrosion.

The surface layer with highest hardness (22.6 % dilution) has the most shallow erosion trench, however of the other four surface layers that have similar hardness, the three with lower dilution have similar erosion depth, while the surface layer with 16.9 % dilution had a better result in the erosion test.

These results coincide with the abrasion tests under dry condition, which leads to the conclusion that the erosion-corrosion mechanism is dominated by abrasive damage: Through the incident angle of the accelerated particles, abrasion is more intense for the surface layers with 2.0 %, 3.3 % and 3.5 % dilution that comprise a – in comparison to the surface layers with higher dilution – softer ferritic-austenitic microstructure in the fusion zone. For 16.9 % dilution, carbide particles in the austenitic matrix increase the abrasion resistance and the carbide network at 22.6 % dilution has the most shallow erosion trench, i.e. the highest resistance. A corrosive component that would e.g. selectively dissolve the austenite grains at the phase boundary to the carbidic phases, did not play any role in this test.

6 Conclusions

Gas metal arc surface welding and plasma transferred arc surface welding at different preheating temperatures were used to prepare surface layers of duplex stainless steel on grey cast iron. The resulting fusion zones had different amounts of chemical dilution and experienced different cooling conditions according to the welding process and preheating temperatures. This lead to a variety of microstructures in the fusion zones which were investigated by metallographic means. Preheating increased the dilution and reduced the cooling rates. This lead to a higher amount of available carbon and increased diffusion in the fusion zones, which resulted in carbide precipitates. For low dilutions and high cooling rates, the microstructure of the fusion zone was ferritic-austenitic. This microstructure seems to be very sensitive to heat input, as for dilutions of 3.5 % there were sometimes already carbides at the austenite-ferrite interfaces in the fusion zone that were "treated" by a more broadened arc of the gas metal arc welding torch as compared to the plasma column, *Figure 12*. For
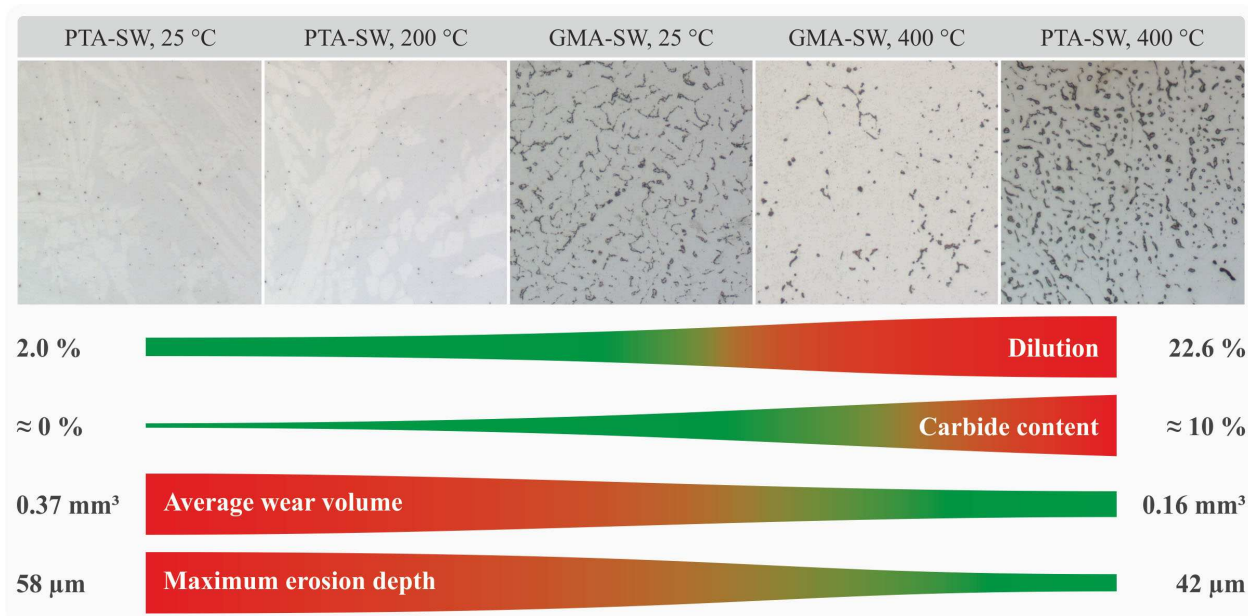
Figure 12. Overview of the microstructures in the fusion zone of the surface layers prepared with plasma transferred arc surface welding and gas metal arc surface welding at different preheating temperatures. The color and thickness of the bars below provide an assessment of the dilution, carbide content, average wear volume and maximum erosion depth (green = better, red = worse, thicker = higher values, thinner = lower values).

higher dilutions and slower cooling rates, these carbides grew in an austenitic matrix (that dissolves less chromium than ferrite in the first place) and eventually connected into a network.

Considering the wear behavior, higher dilution and the precipitation of carbide particles in the austenitic matrix and especially the carbide network seems advantageous, as solid solution hardening, dispersion hardening and the support of a hard-phase network take effect in reduction of the wear volume in the oscillation test as well as in an increase in erosion-corrosion resistance, Figure 12. The fusion zones with a ferritic-austenitic microstructure – though having partly similar hardness values – show increased wear volumes and erosion trench depths.

Studies of the corrosion behavior of the layers that were conducted in parallel and reported elsewhere have shown that increased chemical dilution and carbide precipitates lead to drastic reduction of the corrosion resistance [15, 7]. However, the resistance against erosion-corrosion increased with increasing dilution and heat input due to solid solution hardening, dispersion hardening and the formation of an interconnected network of σ-phase and carbides. This leads to a conflict of interests

between surface layers with excellent corrosion resistance with relatively worse wear properties against surface layers with better wear properties but worse corrosion resistance. Considering the thickness of several millimetres as a wear reserve of the surface layers that could – if needed – be even increased by overlay welding, a sufficient corrosion resistance might be a better compromise if there are operation downtimes or more aggressive media.

This puts the surface layers with low dilution and moderate cooling conditions in favor. In this case, moderate cooling conditions refers to plasma transferred arc surface welding with up to 200 °C preheating temperature as opposed to gas metal arc surface welding without preheating temperature. The surface layer prepared with the latter process already proved that it can provide very good corrosion resistance, however the heat affected zone cracked due to extensive martensite formation that occurred in the (too) rapid cooling of the surface layer.

It needs to be considered that the measured hardness of HV 5 produced rather large indentations, which means that it was fine to get an overview of the general differences between the

surface layers and the influence of the welding processes and preheating temperatures on the respective zones. However, to understand and conclusively explain the observed differences in the wear behavior, microhardness measurements are necessary. Therefore, hardness mapping over the different phases with nanoindentation that only probes one single phase at a time seems very appropriate.

7 Summary

In the present study, the influence of preheating during surface welding of duplex stainless steel with gas metal arc welding and plasma transferred arc welding on grey cast iron substrate on the dilution and microstructure in the fusion zones and the wear behavior under oscillatory loading and exposure to erosive-corrosive conditions of the resulting surface layers was investigated.

The dilution and diffusion that both increased with preheating temperature lead to reduced wear explained by dispersion hardening by precipitation of σ-phase and carbides and formation of a carbide network that supported the structure with highest dilution. It was shown how the dilution influences the chromium and nickel equivalents and their ratio and therefore the solidification mechanisms. However, preheating reduces the cooling rates, which enhances the diffusion of carbon and therefore supports solid state transformation of ferrite to austenite as well as the precipitation of carbides and σ-phase during cooling. Eventually, this enhanced diffusion resulted in a microstructure that had a higher resistance against abrasion and erosion.

As the corrosion behavior has to be considered for the industrial application of surface welding, a lower wear resistance with the advantage of higher corrosion resistance that an evenly distributed ferritic-austenitic microstructure offers, seems to be the better compromise.

The hardness measurements with HV 5 do not suffice to conclusively explain the results of the wear tests, thus, further investigation of the microhardness of the individual phases is performed with use of nanoindentation and microhardness. Future works might also consider laser beam powder surface welding to produce surface layers with even higher cooling rate.

8 References

[1] A. Robinson, S. Bonell, *World Pumps* **2010**, *2010*, 42.

[2] TMR Stainless, Pittsburgh, PA (USA), *Verarbeitung nichtrostender Duplexstähle - Ein praktischer Leitfaden,* 1st ed., International Molybdenum Association, London **2011**.

[3] P. Dupont, M. Cugal, *Sulzer Tech. Rev.* **2006**, *88*, 22.

[4] M. Martins, L.C. Casteletti, *Mater. Charact.* **2009**, *60*, 150.

[5] D.R. Askeland, *Materialwissenschaften: Grundlagen, Übungen, Lösungen*, Springer, Heidelberg **1996**.

[6] V. Muthupandi, P. Bala Srinivasan, S.K. Seshadri, S. Sundaresan, *Mater. Sci. Eng. A* **2003**, *358*, 9.

[7] M. Oechsner, G. Andersohn, J. Ellermeier, B. Heider, U. Reisgen, R. Sharma, S. Wieland, E. Gonzales Olivares, presented at *International Thermal Spray Conference,* Orlando, FL, May 7-10, **2018**, pp. 647-654.

[8] A. Karl, *Dissertation,* Technische Universität Ilmenau, **09/2013**.

[9] P.F. Mendez, N. Barnes, K. Bell, S.D. Borle, S.S. Gajapathi, S.D. Guest, H. Izadi, A.K. Gol, G. Wood, *Journal of Manufacturing Processes,* **2014**, *16*, 4.

[10] E.M. El-Banna, *Mater. Lett.* **1999**, *41*, 20.

[11] E.M. El-Banna, M.S. Nageda, M.M. Abo El-Saadat, *Mater. Lett.* **2000**, *42*, 311.

[12] O. Durst, J. Ellermeier, T. Troßmann, C. Berger, *Materialwiss. Werkstofftech.* **2009**, *40*, 756.

[13] U. Depner, J. Ellermeier, T. Troßmann, C. Berger, M. Oechsner, *Int. J. Mater. Res.* **2011**, *102*, 1014.

[14] K. Bobzin, L. Zhao, M. Öte, T. Königstein, M. Oechsner, M. Siebers, G. Andersohn, J. Ellermeier, *Materialwiss. Werkstofftech.* **2017**, *48*, 922.

[15] U. Reisgen, K. Willms, S. Wieland, E. Gonzales, M. Oechsner, J. Ellermeier, M. Siebers, B. Heider, *Materialwiss. Werkstofftech.* **2018**, *49*, 1520.

[16] F. Iacoviello, F. Casari, S. Gialanella, *Corros. Sci.* **2005**, *47*, 909.

[17] E. Folkhard, G. Rabensteiner, *Welding metallurgy of stainless steels*, Springer-Verlag, Wien, New York **1988**.

[18] M. Knyazeva, M. Pohl, *Metallogr. Microstruct. Anal.* **2013**, *2*, 343.

[19] P.L. Ferrandini, C.T. Rios, A.T. Dutra, M.A. Jaime, P.R. Mei, R. Caram, *Mater. Sci. Eng. A* **2006**, *435*, 139.

[20] K. Rajasekhar, C.S. Harendranath, R. Raman, S.D. Kulkarni, *Mater. Charact.* **1997**, *38*, 53.

[21] A.L. Schaeffler, *Met. Prog.* **1949**, *56*, 680.

[22] M. Knyazeva, M. Pohl, *Metallogr. Microstruct. Anal.* **2013**, *2*, 113.

[23] Düker GmbH & Co. KGaA, Gusseisen mit Lamellengrafit EN-GJL-150 bis 350.

[24] Castolin Eutectic, EuTroLoy 16462: Metallpulver für korrosionsbeständige Beschichtungen **03/2014**.

[25] voestalpine Böhler Welding GmbH, Thermanit 22/09: Massivdraht, hochlegiert, rostfrei **05/2014**.

[26] Deutsche Edelstahlwerke GmbH, Acidur 4462: Werkstoffdatenblatt X2CrNiMoN22-5-3 **10/2015**.

[27] S. Selvi, A. Vishvaksenan, E. Rajasekar, *Def. Technol.* **2018**, *14*, 28.

[28] J. Ellermeier, *Dissertation,* RWTH Aachen, **05/1996**.

[29] U. Dilthey, J. Ellermeier, A.V. Pavlenko, *Schweißen und Schneiden* **1996**, *47*, 227.

[30] DIN Deutsches Institut für Normung e. V., *9015-2:***2016-10**.

[31] DIN Deutsches Institut für Normung e. V., *9015-1:***2011-05**.

[32] MESYS AG, https://www.mesys.ch/?page_id = 54, accessed: August 2, 2018.

[33] DIN Deutsches Institut für Normung e. V., *51834-2:***2010-11**.

[34] DIN Deutsches Institut für Normung e. V., *51834-3:***2008-12**.

[35] O. Durst, J. Ellermeier, T. Troßmann, C. Berger, *Materialwiss. Werkstofftech.* **2009**, *40*, 756.

[36] DIN Deutsches Institut für Normung e. V., *50905-4:***2018-03**.

[37] U. Depner-Miller, J. Ellermeier, H. Scheerer, M. Oechsner, K. Bobzin, N. Bagcivan, T. Brögelmann, R. Weiss, K. Durst, C. Schmid, *Surf. Coat. Technol.* **2013**, *237*, 284.

[38] I. Mitelea, I.-D. Utu, S.D. Urlan, C.M. Crăciunescu, *Materialwiss. Werkstofftech.* **2017**, *48*, 1040.